Superwettable Dendritic Gold Nanostructured Electrode Arrays for Electrochemical Enzyme-Linked Immunosorbant Assay (ELISA)

Ping Fang[1], Jishun Li[1], Fuyang Jiang[1], Jianfeng Meng[2,*] and Hongcheng Pan[1,3,*]

[1] College of Chemistry and Bioengineering, Guilin University of Technology, 12 Jiangan Road, Guilin, P. R. China
[2] Department of Respiratory and Critical Care Medicine, the People's Hospital of Guangxi Zhuang Autonomous Region, 6 Taoyuan Road, Nanning, P. R. China
[3] Guangxi Key Laboratory of Electrochemistry and Magnetochemistry Functional Materials, Guilin University of Technology, 12 Jiangan Road, Guilin, P. R. China
*E-mail: panhongcheng@glut.edu.cn

Hydrophobic/hydrophilic patterning on dendritic gold nanostructures (Au-DNs) provides an attractive platform for biosensing. However, the rapid fabrication of superwettable Au-DNs without hydrophobic molecular modifications remains highly challenging. Here, we used a simple heating method to convert Au-DNs electrodeposited on indium tin oxide (ITO)-coated glass from superhydrophilic to superhydrophobic. Nine gapped rings (each with a diameter of 2 mm, width of 160 μm, and gap of 0.5 mm) were etched on the superhydrophobic Au-DNs/ITO electrode (2 cm × 3 cm) with a laser engraver. The laser-etched rings are hydrophilic and combine with the enclosing superhydrophobic regions to form superwettable microwells that serve as an array of working electrodes. The superwettable Au-DNs/ITO electrode arrays were used as the working electrode for electrochemical enzyme-linked immunosorbant assay (ELISA) detection of human immunoglobulin (IgG). In the electrochemical ELISA, the capture antibody (goat anti-human IgG) was immobilized onto the Au-DNs/ITO electrode, and the labeled antibody was labeled with horseradish peroxidase. After the immunoreaction, 10 μL of droplets containing hydrogen peroxide were added to the superwettable microwells. Differential pulse voltammetry was used to measure the peak currents of the droplets at approximately -0.07 V. The calibration curve of peak current intensity versus IgG concentration is linear in the range of 5-250 ng/mL, with a detection limit of 3.61 ng/mL. The electrochemical immunosensor exhibits high selectivity, reproducibility and recovery, and was applied to detect IgG in real serum samples, demonstrating its promising application in clinical diagnosis.

1. INTRODUCTION

Dendritic gold nanostructures (Au-DNs) are a type of hyperbranched structure characterized by long primary trunks, parallel secondary or tertiary branches with sharp edges or tips, and nanoscale gaps [1-6]. Au-DNs can provide a promising platform for the design and construction of functional sensors, due to their large surface area, distinctive shapes, and high activity [7-9]. Au-DNs have been developed as active substrates for surface-enhanced Raman scattering (SERS) because they can form many "hot spots" at the tips of branches or in the nanogaps between adjacent branches [10-12]. Au-DNs exhibit a high catalytic activities toward the nonenzymatic oxidation/reduction of glucose and hydrogen peroxide, which enables their use in electrochemical sensors [13, 14]. Using dendritic nanogold modified electrodes, our group developed a sensitive electrochemical sensor for selenium and copper [15].

Previous research has demonstrated that dendritic gold-modified electrodes can detect biomolecules with high sensitivity [16, 17]. Chiles and coworkers developed an electrochemical enzyme-linked immunosorbant assay (ELISA) based on dendritic gold-modified electrodes for the detection of cholera toxin subunit B [16]. Nayak et al. used an electrochemical immunosensor based on hyperbranched gold nanostructures to detect epithelial growth factor receptor protein at a concentration of pg/mL [18]. However, electrochemical biosensing using Au-DNs modified electrodes is typically performed in a large-volume solution, which may result in the waste of expensive reagents or samples.

Superwettable microchips, also known as superhydrophilic-superhydrophobic patterns, have recently been used to control and pattern droplets as microelectrochemical cells in electrochemical biosensing [19]. Wang and colleagues developed a superwettable microchip by modifying dodecanethiol on electrodeposited Au-DNs films to generate superhydrophobic surfaces. The superhydrophobic surfaces were then irradiated with oxygen plasma via a photomask to produce superhydrophobic-superhydrophilic micropatterns [20]. Electrochemical detection was performed in microdroplets anchored in superhydrophilic microwells via capillary forces. The microwell surface was preimmobilized with redox-reporter-modified DNA probes or aptamers for the detection of prostate cancer biomarkers (miRNA-375, miRNA-141, and prostate-specific antigen).

The formation of superwettable surfaces on Au-DNs-modified substrates is critical. To obtain hydrophobic/hydrophilic patterns, it is necessary to self-assemble hydrophobic molecules containing alkane chains (or fluoroalkyl) on Au-DNs. Photomasks are also required when using oxygen plasma to etch the hydrophobic surfaces. However, for most electrochemical biosensing, it is preferable to obtain clean Au-DNs superhydrophobic surfaces without hydrophobic molecules. A clean surface is beneficial for minimizing interference. Moreover, the use of photomasks limits rapid structuring in prototype device development, and the cost of high-resolution photomasks is too high for the fabrication of individual sensor devices.

Here, we present a superwettable Au-DNs-based electrode array that does not require the use of hydrophobic molecules or photomasks. A simple heating method was used to convert the superhydrophilicity of Au-DNs electrodeposited on indium tin oxide (ITO)-coated glass to superhydrophobicity. Using a laser engraver, nine gapped rings (each with a diameter of 2 mm, width of 160 μm, and gap of 0.5 mm) were etched directly onto a superhydrophobic Au-DNs/ITO electrodes (2

cm×3 cm). The laser-etched rings are hydrophilic and combine with the enclosing superhydrophobic regions to form superwettable microwells that serve as an array of working electrodes. We applied the superwettable Au-DNs/ITO electrode arrays to electrochemical ELISA. The human immunoglobulin (IgG)/horseradish peroxidase (HRP)-labeled goat anti-human IgG antibody system was selected as the model system to optimize the methodology. A drop of 10 μL solution containing hydrogen peroxide was added onto a superwettable microwell for electrochemical ELISA detection. The Au-DNs/ITO electrode arrays can provide an excellent platform for antibody immobilization and immune reactions, and exhibit a sensitive response to hydrogen peroxide, allowing for electrochemical ELISA in a microliter-scale droplet. Moreover, the microarray electrode can measure multiple samples with varying concentrations on a single electrode or perform a multiplexed assay, significantly increasing reproducibility and efficiency.

2. EXPERIMENTAL SECTION

2.1 Chemicals and instruments

Goat anti-human IgG antibody (Ab1), horseradish peroxidase labeled goat anti-human IgG antibody (HRP-Ab2), and bovine serum albumin (BSA) were purchased from Bomei Biotechnology (Hefei, China). Human serum samples were obtained from Kejing Biotechnology (Jiangsu, China). $HAuCl_4 \cdot 4H_2O$ was obtained from Sinopharm Reagent (Beijing, China). $Na_2HPO_4 \cdot 12H_2O$, $NaH_2PO_4 \cdot 2H_2O$, HNO_3, KCl, CH_3CH_2OH, and CH_3COCH_3 were obtained from Xilong Chemical (Shantou, China). 3-Mercaptopropyltrimethoxysilane (MPTMS) was obtained from Tairui New Material (Guangzhou, China). ITO-coated glass (square resistance < 7 ohm/sq, transmittance ≥ 77%, thickness = 1.1 mm) was obtained from Kaivo Optoelectronic Technology (Zhuhai, China). All chemicals employed in this experiment were analytical grade reagents. Ultrapure water (resistivity > 18 MΩ cm) was obtained from a Milli-Q purification system (Millipore, USA).

Electrochemical experiments were carried out with a CHI660B electrochemical workstation (Chenhua Instruments, Shanghai, China). Etching of the Au-DNs/ITO electrode arrays was performed by a laser engraver (ET650IR, Tuopu silver optoelectronic technology, Wuhan, China). Contact angles were measured using an optical contact angle goniometer. (JC2000D1, Zhongchen digital technology, Shanghai, China). The morphology and composition of Au-DNs were analyzed by a scanning electron microscopy (SEM) (SU5000, Hitachi, Tokyo, Japan) equipped with an energy dispersive X-ray spectrometer (EDS). The crystal structure of Au-DNs was characterized by powder X-ray diffraction (XRD, X'Pert3Powder, Panaco, Netherlands).

2.2 Pretreatment of ITO electrodes

The ITO-coated glasses were cut into small rectangular pieces (2 cm × 3 cm), and washed with acetone, ethanol, and ultrapure water for 5 min to remove surface impurities. Subsequently, the ITO electrodes were placed in a drying oven and dried at 60 °C for 0.5 h. To enhance the adhesion to Au-

DNs, the ITO electrodes were mercapto-silylated in a 1% (v/v) MPTMS ethanol solution for 1 h, washed with ethanol and ultrapure water, and dried in air before use.

2.3 Preparation of superwettable Au-DNs/ITO electrode arrays

A schematic of preparation of superwettable Au-DNs/ITO electrode arrays is illustrated in Figure 1A. First, Au-DNs were electrodeposited on ITO electrodes in a 10-mL solution containing 0.1% (w/w) chloroauric acid and 0.9 M HNO_3 at a constant potential of -1.8 V for 5400 s using the ITO electrode, a saturated Ag/AgCl electrode, and a platinum plate as the working, reference, and counter electrodes, respectively. Then the Au-DNs/ITO electrodes were heated at 120 °C for 3 h to reverse the surface state from superhydrophilic to superhydrophobic. Nine gapped rings (each with a diameter of 2 mm, width of 160 μm, and gap of 0.5 mm) were laser-etched onto each Au-DNs/ITO electrode. The hydrophilic rings combine with the enclosing superhydrophobic regions to form superwettable microwells that serve as a 3×3 array of working electrodes.

2.4 Fabrication of the electrochemical immunosensors based on the Au-DNs/ITO electrode arrays

The immunosensor fabrication involves a typical sandwich ELISA procedure, as depicted in Figure 1B. First, 5 μL of 10 μg/mL Ab1 solution was added to each microwell of an Au-NDs/ITO electrode, incubated at 37°C for 2 h, and rinsed repeatedly with 0.2 M phosphate-buffered saline (PBS, pH 7.4) solution (hereafter referred to as Ab1/Au-NDs/ITO). After that, 5 μL of 0.1% (w/w) BSA solution was added to each microwell and incubated for 2 h at 37°C to prevent nonspecific protein adsorption (hereafter referred to as BSA/Ab1/Au-NDs/ITO). For the detection of IgG, 5 μL of IgG solution (or sample) containing various concentrations was added to each microwell, incubated at 37°C for 1 h, and washed with 0.2 M PBS solution to remove weakly adsorbed IgG (hereafter referred to as IgG/BSA/Ab1/Au-NDs/ITO). Finally, 5 μL of Ab2-HRP solution was added to each microwell, incubated at 37°C for 1 h, and washed three times with 0.2 M PBS solution (hereafter referred to as Ab2-HRP/IgG/BSA/Ab1/Au-NDs/ITO).

2.5 Electrochemical ELISA for the detection of IgG

To detect IgG by electrochemical ELISA, a drop of 10 μL of 0.1 M hydrogen peroxide solution was added to each microwell of the Ab2-HRP/IgG/BSA/Ab1/Au-NDs/ITO electrode. A platinum wire (0.3 mm in diameter) was attached to an Ag/AgCl microreference electrode (1.5 mm in bottom tip diameter) and inserted into the droplet on the microwell, while avoiding direct contact with the surface. The peak current intensity between -0.3 V and 0.2 V was measured using differential pulse voltammetry (DPV) with a pulse width of 0.05 V, a pulse width of 0.05 s, and a pulse period of 0.2 s.
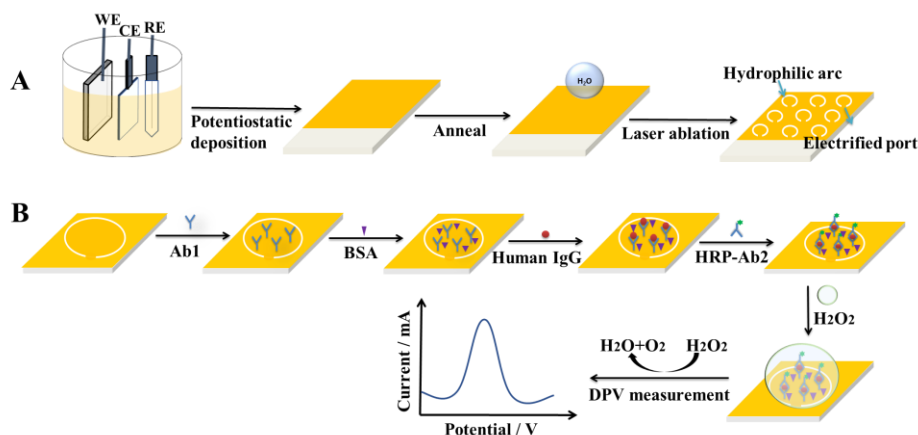
Figure 1. (A) Preparation of superwettable Au-DNs/ITO electrode arrays; (B) Schematic diagram of the electrochemical ELISA using Au-DNs/ITO electrode arrays.

3. RESULTS AND DISCUSSION

3.1 Morphology, composition, and structure composition of Au-NDs

The morphology and composition of Au-DNs electrodeposited on ITO glasses were characterized by SEM and EDS. As illustrated in Figure 2A and 2B, the ITO substrates are covered with densely hierarchical dendritic nanostructures whose primary, secondary, and tertiary branches having respectively lengths of 10-18 μm, 4-5 μm, and 0.3-1.2 μm, and diameters of 0.6-1.0 μm, 100-300 nm, and 100-200 nm.
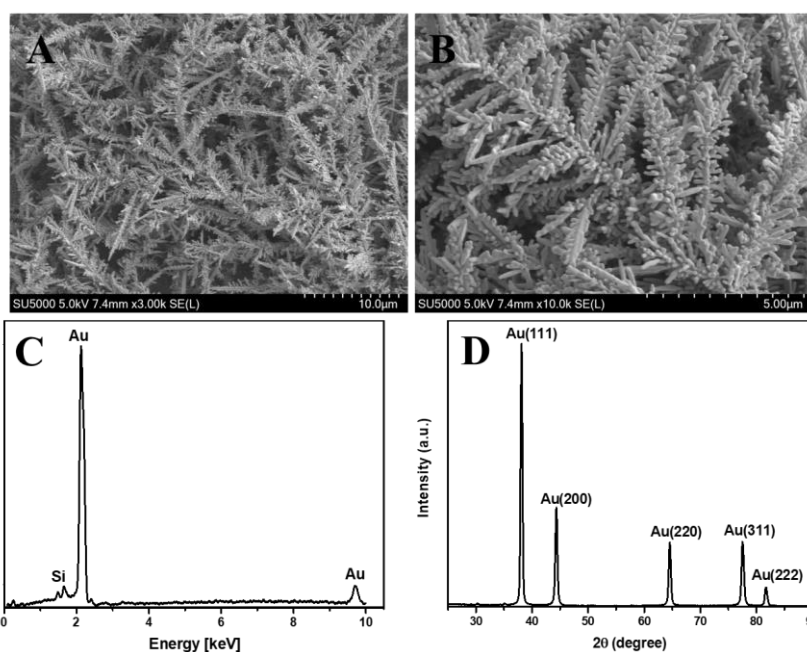

Figure 2. SEM images at 3 k (A) and 10 k (B) magnification, EDS spectrum (C), and XRD spectrum (D) of Au-DNs.

The EDS spectrum in Figure 2C reveals that the dendritic nanostructure is entirely composed of Au, and a small Si peak in the spectrum originates from the ITO substrate. XRD studies provide further details about the crystal structure of Au-DNs (Figure 2D). Five sharp and strong diffraction peaks were identified at 38.1°, 44.4°, 64.6°, 77.5°, and 81.7°, corresponding to the (111), (200), (220), (311), and (222) planes of face-centered cubic (FCC) Au (JCPDF NO.01-089-3697), respectively. The XRD results indicate that Au-DNs have a relatively high crystallinity.

3.2 Characterization of wettability of electrode surface

The wettability of various electrode surfaces was evaluated by contact angle measurements, as illustrated in Figure 3. The water contact angle of a bare ITO substrate is approximately 56.64° (Figure 3A). The electrodeposition of Au-DNs on the ITO substrate reduced the contact angle to 2.79° (Figure 3B), indicating that the Au-DNs/ITO electrode is superhydrophilic.
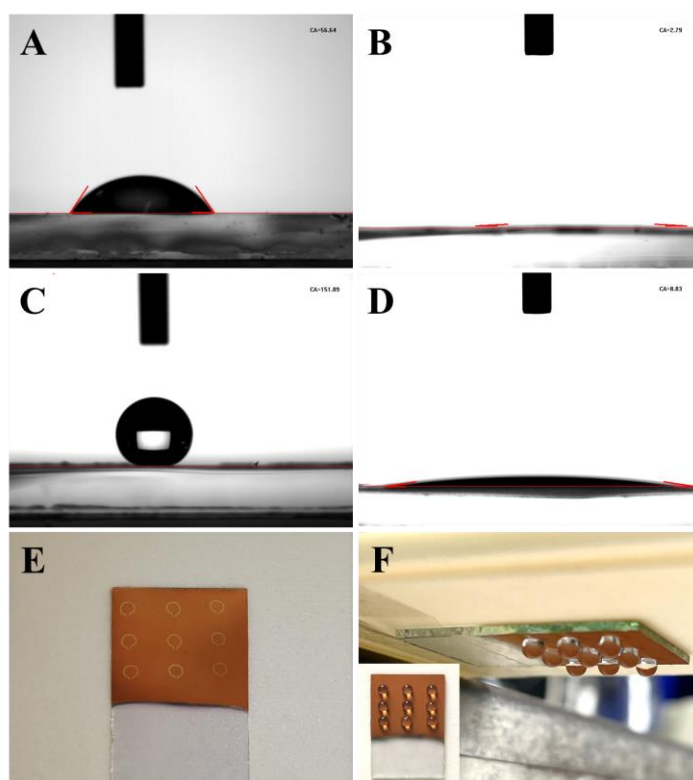

Figure 3. Water contact angle of (A) bare ITO, Au-DNs/ITO electrode (B) without heating treatment and (C) after heating at 120°C for 3 h, (D) laser-etched surface of Au-DNs/ITO electrode, and superwettable microwells on Au-DNs/ITO electrode (E) with and (F) without water droplets.

According to previous studies, clean gold surfaces are naturally hydrophilic and may form a water film composed of tens of molecular layers. Hieratical dendritic gold nanostructures have rough surfaces and large contact areas, which further increase the hydrophilicity of the Au-DNs/ITO electrode to superhydrophilicity. After the Au-DNs/ITO electrode was heated at 120°C for 3 h, the water contact

angle increased by 149° to 151.89° (Figure 3C). Similarly, Ren et al. observed a thermally-induced transition from superhydrophilicity to superhydrophobicity when ozone-treated carbon nanotubes were heated to 600°C [21]. Heating is believed to evaporate the most of physically adsorbed water molecules, thereby increasing the contact angle [22]. Once the contact angle exceeds a critical value (90°), according to the Cassie–Baxter model, the rough surface of Au-DNs can significantly reduce the cosine value of the apparent contact angle, resulting in a superhydrophobic surface [22, 23]. After laser etching of the superhydrophobic Au-DNs/ITO electrode, the etched surface became hydrophilic with a contact angle of 8.83%, as shown in Figure 3D. Figure 3E shows a superhydrophobic Au-DNs/ITO electrode etched with a 3×3 array of gapped rings. These hydrophilic gapped rings combine with the enclosing superhydrophobic regions to form superwettable microwells capable of anchoring droplets. As seen in Figure 3F, nine water droplets (10 µL each) were firmly anchored to the 3×3 array of gapped rings and did not fall off even when the electrode was inverted at 180°.

3.3 Electrochemical characterization of the electrochemical immunosensor

Electrochemical impedance spectroscopy (EIS) can provide more detailed information about the properties of the electrode interface. The impedance spectrum consists of a semicircle at high frequencies, corresponding to the electron transfer limitation process, and a line at low frequencies, resulting from the diffusion limitation step of the electrochemical process. We used the EIS to monitor the stepwise fabrication process of the electrochemical immunosensor. The semicircular diameter of the EIS corresponds to the charge transfer resistance at the electrode interface at each step of the electrode fabrication process. Figure 4A shows the EIS of the electrodes at different stages of fabrication in a 0.1 M KCl solution containing 5 mM $[Fe(CN)_6]^{3-/4-}$ solution. For the bare Au-NDs/ITO electrodes, the semicircle diameter is only 73.26 Ω (curve a). Electrochemically deposited hierarchical dendritic gold microstructure with secondary and tertiary branches may play a significant role similar to that of wires or electron conduction tunnels, thereby facilitating electron transfer [24]. The semicircular diameter increased significantly after immobilizing Ab1 on the Au-NDs/ITO electrode (curve b). These results indicate that the antibodies formed an insulating layer on the electrode surface, increasing resistance and impeding electron transfer. In subsequent steps, blocking the electrode with BSA and adding IgG resulted in a continuous increase in the semicircular diameter (curves c and d), implying the formation of antigen-antibody complexes that further impede electron transfer. A significant increase in semicircular diameter was observed with the addition of Ab2-HRP (curve e), which can be explained by the formation of a thick HRP-Ab2/IgG/Ab1 sandwich immune complex layer.

Cyclic voltammetry (CV) was also used to characterize the electrode interface at each step. The experimental results of cyclic voltammetry are very similar to those of EIS (Figure 4B). The greatest decrease in peak current was observed during the step of immobilizing Ab1 on the Au-DNs/ITO electrode. During the subsequent antigen-antibody binding step, the peak current gradually decreases. Similar experimental phenomena were also observed during the assembly of other electrochemical immunosensors [25, 26]. The assembly of insulating protein layers generally leads to a decrease in CV

peak current and an increase in charge transfer resistance. Both our EIS and CV results support the successful assembly of the electrochemical ELISA sensor.
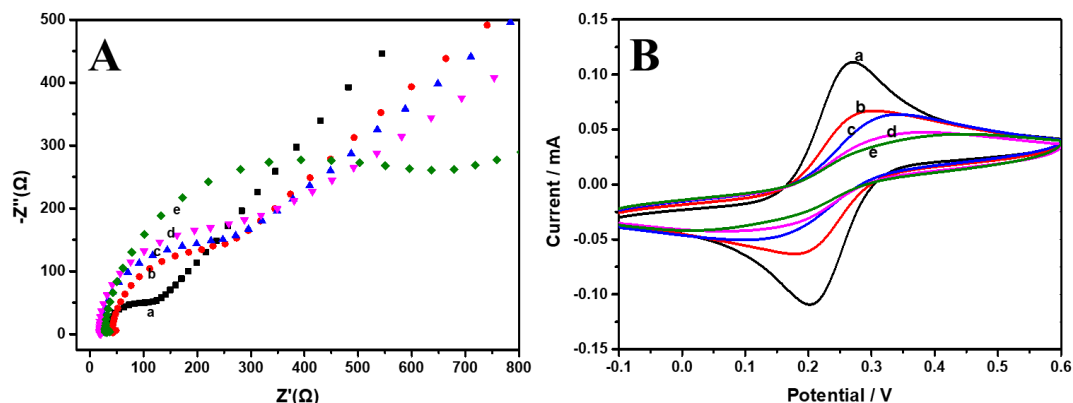

Figure 4. EIS (A) and CV (B) of different modified electrodes in 5 mM $[Fe(CN)_6]^{3-/4-}$ solution: (a) Au-DNs/ITO, (b) Ab1/Au-DNs/ITO, (c) BSA/Ab1/Au-DNs/ITO, (d) IgG/BSA/Ab1Au-DNs/ITO, (e) HRP-Ab2/IgG/BSA/Ab1/Au-DNs/ITO electrodes.

3.4 Optimization of the analytical conditions

We optimized important experimental parameters that could affect the sensor performance, including pH value, reaction time for HRP-catalyzed H_2O_2 decomposition, H_2O_2 concentration, incubation time, and HRP-Ab2 concentration. The pH value has a significant influence on the binding of antigen-antibody and catalytic activity. As shown in Figure 5A, the maximum peak current occurred at a pH of 7.4, and thus the optimal pH value was determined to be 7.4.

The reaction time required for HRP-catalyzed H_2O_2 decomposition has a direct effect on the magnitude of the DPV peak current. Insufficient reaction time results in decreased H_2O_2 catalysis efficiency, whereas an extended reaction time may result in a lower peak current due to excessive H_2O_2 consumption. As shown in Figure 5B, the peak current is maximum at a reaction time of 1 min and rapidly decreases with increasing reaction time. Then, the optimal reaction time was determined to be 1 min. The effect of H_2O_2 concentration on the peak current was also investigated. The peak current intensity increased considerably when the H_2O_2 concentration exceeded 0.06 M. After the H_2O_2 concentration reached 0.08 M, the peak current increased gradually and reached its maximum value at 0.1 M. A further increase in the H_2O_2 concentration resulted in a slight decrease in the peak current. This is most likely because the high concentration of H_2O_2 impedes the catalytic reaction of HRP [27]. The optimal H_2O_2 concentration was determined to be 0.1 M (Figure 5C). We investigated the effect of HRP-Ab2 concentration and incubation time on peak currents. As shown in Figure 5D and 5E, the optimal HRP-Ab2 concentration and incubation time are 10 μg/mL and 60 min, respectively.
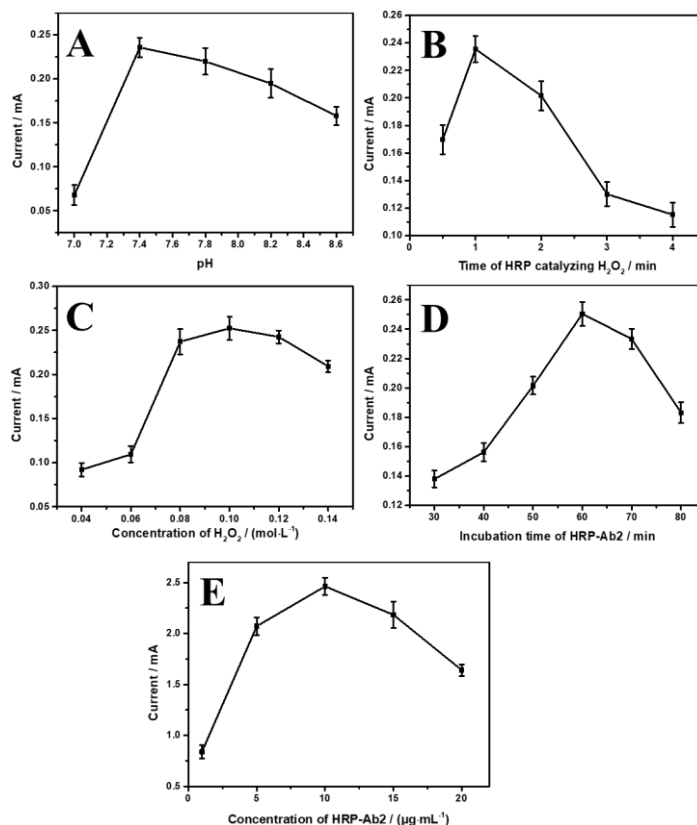
Figure 5. Optimization of the analytical conditions: (A) pH value; (B) reaction time of HRP-catalyzed H_2O_2 decomposition; (C) H_2O_2 concentration; (D) HRP-Ab2 incubation time; (E) HRP-Ab2 concentration. (Error bars represent relative standard deviations for three independent measurements).

3.5 Analytical performance of the electrochemical immunosensor

Under optimal experimental conditions, the performance of the electrochemical immunosensor was further evaluated for the detection of human IgG.
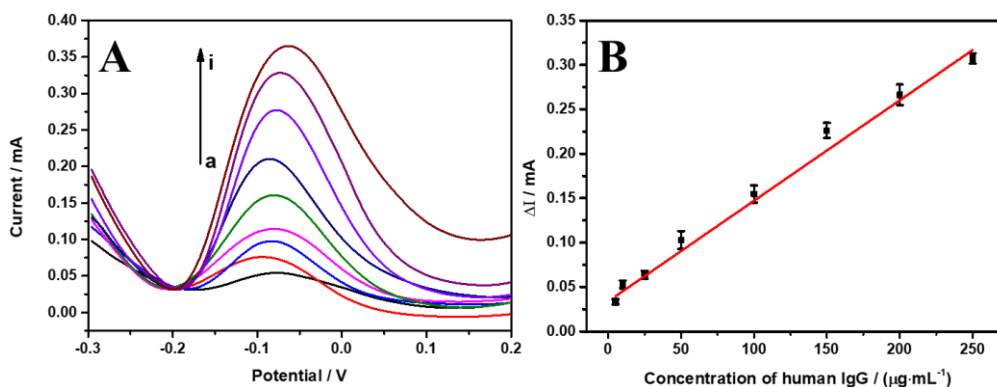

Figure 6. (A) DPV curves of the immunosensor after incubation with different concentrations of IgG, a-i , 0, 5, 10, 25, 50, 100, 150, 200, and 250 ng/mL; (B) calibration plot. (Error bars represent relative standard deviations for three independent measurements).

The DVP curves of the immunosensor with increasing IgG concentrations are shown in Figure 6A (from bottom to top: 0, 5, 10, 25, 50, 100, 150, 200, 250 ng/mL), exhibiting that the peak current intensity increases as the human IgG concentration increases. The calibration plot shown in Figure 6B shows a significant linear relationship between the peak current and the human IgG concentration. A linear regression equation for IgG in the concentration range of 5-250 ng/mL was found to be $\Delta I = 0.00113 \, C_{IgG} + 0.03399$ with a correlation coefficient of 0.990, and a limit of detection of 3.61 ng/mL (3δ).

3.6 Selectivity and reproducibility of the immunosensor

We evaluated the selectivity of the immunosensor using electroactive substances commonly found in serum (ascorbic acid and glucose) and the most abundant protein (albumin) in serum as interferents. As illustrated in Figure 7, the variation in the peak current intensity for detecting human IgG (50 ng/ml) is less than 5% in the presence of ascorbic acid, glucose, and albumin (500 ng/ml each), indicating that the immunosensor has good selectivity. We evaluated the reproducibility of the electrochemical immunosensor by measuring the same concentration of IgG solution (150 ng/mL) on six Au-DNs/ITO electrodes under optimized conditions. The relative standard deviation (RSD) of the peak currents was 4.73%, indicating that the electrochemical immunosensor is highly reproducible.
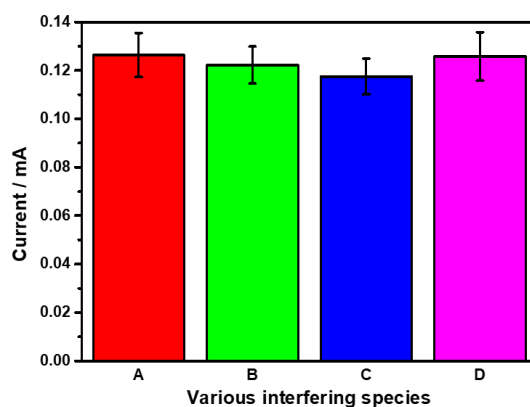

Figure 7. Selectivity of the electrochemical immunosensor: (A) 50 ng·mL^{-1} IgG, (B) 50 ng·mL^{-1} IgG + 500 ng·mL^{-1} Glucose, (C) 50 ng·mL^{-1} IgG + 500 ng·mL^{-1} VC, (D) 50 ng·mL^{-1} IgG + 500 ng·mL^{-1} BSA. (Error bars represent relative standard deviations for three independent measurements)

3.7 Analysis of real samples

To evaluate the applicability of the immunosensor in real sample detection, we performed serum sample detection and spike recovery experiments. After appropriate dilution and under optimal analytical conditions, human serum samples were used to detect the IgG concentration. Spiked recovery experiments were performed on serum samples at two concentrations of 50 and 100 ng/mL, with five serum samples taken for each concentration. The recoveries and relative standard deviations (RSDs) of

the assay values were calculated and the results are summarized in Table 1. The results demonstrated that the developed immunosensor can be applied to the detection of real samples with excellent analytical capability as the recoveries ranged from 98.55-105.20% with RSDs less than 10%.

Table 1. Recoveries and RSDs for IgG detection in human serum samples

Samples	Detected (ng/mL)	Added (ng/mL)	Found (ng/mL)	Recovery (%)	RSD (%, n=5)
serum samples	9.38	50.00	61.98	105.20	6.52
		100.00	107.93	98.55	8.98

4. CONCLUSION

The superwettable Au-DNs-based electrode arrays can be rapidly fabricated using a laser engraver without the use of hydrophobic molecules or photomasks. Superwettable dendritic gold has a large surface area and an excellent ability to anchor droplets. It is an excellent platform for antibody immobilization and immune reactions, and its sensitivity to hydrogen peroxide enables electrochemical ELISA in microliter-scale droplets. Additionally, the electrode arrays can measure multiple samples with varying concentrations on a single electrode or perform multiple detection, significantly improving reproducibility and efficiency. The Au-DNs/ITO electrodes were used to develop an electrochemical ELISA immunosensor for detecting human IgG in microliter droplets. The immunosensor was successfully used to detect IgG levels in human serum samples with a detection limit of 3.61 ng/mL and demonstrated excellent selectivity, reproducibility, and recovery. The electrochemical immunosensors also have the advantages of a simple manufacturing process, low cost and ease of mass production, and have numerous potential applications in clinical diagnosis.

References

1.   W.C. Ye, J.F. Yan, Q.A. Ye and F. Zhou, *J. Phys. Chem. C*, 114 (2010) 15617.
2.   G.W. Lu, C. Li and G.Q. Shi, *Chem. Mater.*, 19 (2007) 3433.
3.   D.P. Huang, X.T. Bai and L.Q. Zheng, *J. Phys. Chem. C*, 115 (2011) 14641.
4.   X.L. Xu, J.B. Jia, X.R. Yang and S.J. Dong, *Langmuir*, 26 (2010) 7627.
5.   A.T. Gulderen, Y. Oztekin and J. Barek, *Monatsh. Chem.*, 151 (2020) 1257.
6.   Y. Hu, N. Pan, K. Zhang, Z.X. Wang, H.L. Hu and X.P. Wang, *Phys. Status Solidi A*, 204 (2007) 3398.
7.   J.L. Wang, F.Y. Chen, Y.C. Jin and R.L. Johnston, *J. Mater. Chem. A*, 4 (2016) 17828.

8.   S.J. Yi, L.M. Sun, S.C. Lenaghan, Y.Z. Wang, X.Y. Chong, Z.L. Zhang and M.J. Zhang, *RSC Adv.*, 3 (2013) 10139.
9.   D.D. Shen, Y.C. Liu, Y. Fang, P. Li and Z.S. Yang, *J. Solid State Electrochem.*, 19 (2015) 563.
10.   Y.C. Song, T.L. Xu, L.P. Xu and X.J. Zhang, *Chem. Commun.*, 55 (2019) 1742.
11.   H.Y. Liu, P.N. Zhao, W.L. Xiu, L.N. Zhang, P.H. Zhu, S.G. Ge and J.H. Yu, *Sens. Actuators, B*, 355 (2022) 131264.
12.   T.Y. Xia, H. Luo, S.G. Wang, J.L. Liu, G.H. Yu and R.M. Wang, *CrystEngComm*, 17 (2015) 4200.
13.   E. Rafatmah and B. Hemmateenejad, *Sens. Actuators, B*, 304 (2020) 127335.
14.   A. Sukeri and M. Bertotti, *J. Electroanal. Chem.*, 805 (2017) 18.
15.   H.F. Wang, Y. Guo and H.C. Pan, *Analyst*, 146 (2021) 4384.
16.   A.E. Valera, N.T. Nesbitt, M.M. Archibald, M.J. Naughton and T.C. Chiles, *ACS Sens.*, 4 (2019) 654.
17.   P. Bauer, K. Mougin, D. Faye, A. Buch, P. Ponthiaux and V. Vignal, *Langmuir*, 36 (2020) 11015.
18.   S. Bakshi, S. Mehta, T. Kumeria, M.J. Shiddiky, A. Popat, S. Choudhury, S. Bose and R. Nayak, *Sens. Actuators, B*, 326 (2021) 128803.
19.   T.L. Xu, L.P. Xu, X.J. Zhang and S.T. Wang, *Chem. Soc. Rev.*, 48 (2019) 3153.
20.   T.L. Xu, Y.C. Song, W. Gao, T.T. Wu, L.P. Xu, X.J. Zhang and S.T. Wang, *ACS Sens.*, 3 (2018) 72.
21.   H.Z. Wang, Z.P. Huang, Q.J. Cai, K. Kulkarni, C.L. Chen, D. Carnahan and Z.F. Ren, *Carbon*, 48 (2010) 868.
22.   J. Drelich, E. Chibowski, D.D. Meng and K. Terpilowski, *Soft Matter*, 7 (2011) 9804.
23.   M.J. Liu, S.T. Wang and L. Jiang, *Nat. Rev. Mater.*, 2 (2017) 1.
24.   J. Tang, D.P. Tang, R. Niessner, D. Knopp and G.N. Chen, *Anal. Chim. Acta*, 720 (2012) 1.
25.   S.K. Arya and P. Estrela, *Methods*, 116 (2017) 125.
26.   P.P. Chen, X.X. Hua, J.H. Liu, H.B. Liu, F.Q. Xia, D. Tian and C.L. Zhou, *Anal. Biochem.*, 574 (2019) 23.
27.   Z.M. Liu and H.Y. Wang, *Analyst*, 144 (2019) 5794.